Nano Energy 43 (2018) 310–316

Contents lists available at ScienceDirect

Nano Energy

journal homepage: www.elsevier.com/locate/nanoen

Full paper

Fundamental understanding and rational design of high energy structural microbatteries

Yuxing Wang[a], Qiuyan Li[a], Samuel Cartmell[a], Huidong Li[a], Sarah Mendoza[a], Ji-Guang Zhang[a], Zhiqun Daniel Deng[a], Jie Xiao[a,b,*]

[a] Energy and Environment Directorate, Pacific Northwest National Laboratory, P.O. Box 999, Richland, WA 99352, United States
[b] Department of Chemistry & Biochemistry, University of Arkansas, Fayetteville, AR 72701, United States

ARTICLE INFO

Keywords:
Tube-shape
Lithium batteries
Microbatteries

ABSTRACT

Microbatteries play a critical role in determining the lifetime of downsized sensors, wearable devices, medical applications, and animal acoustic telemetry transmitters among others. More often, structural batteries are required from the perspective of aesthetics and space utilization, which is however rarely explored. Herein, we discuss the fundamental issues associated with the rational design of practically usable high energy microbatteries. The tubular shape of the cell further allows the flexible integration of microelectronics. A functioning acoustic micro-transmitter continuously powered by this tubular battery has been successfully demonstrated. Multiple design features adopted to accommodate large mechanical stress during the rolling process are discussed providing new insights in designing the structural microbatteries for emerging technologies.

1. Introduction

The rapid development in the field of electronic devices continually improves our life as portable devices become more functionalized, more compact and cost less. It is widely recognized that the energy storage devices such as the batteries for powering electronic devices are the limiting components, the energy density of which does not double every two years like components in integrated circuits [1]. Besides the apparent gravimetric/volumetric density limitation, the shape of batteries also limits their efficient integration especially with portable electronic devices. Lithium batteries are the obvious choices in most portable electronic devices for their high energy densities. Conventional lithium batteries are available in coin, pouch or cylindrical-type cells. As the bulkiest components in a device in many cases, batteries can be a nuisance to designers from the aesthetics point of view. The rigidity of battery dimension also greatly hinders the utilization of free space in portable electronic devices.

Recently, there has been great interest in designing batteries that are bendable, twistable and even stretchable [2–4]. These batteries make electronic devices that could respond to large elastic strain a reality, such as wearable devices and rollup display. The key challenges to make batteries flexible include but not limited to lamination, strain management and electrolyte distribution. Those factors are often intertwined. For example, mechanical bending and stretching could induce tensile and compressive strain not only in the electrodes and separator layers but also at the interfaces of electrodes/separator and electrodes/current collectors. Delamination due to excessive strain could lead to poor contact, loss of electrochemical performance and even shorting. Strategies to mitigate these problems in flexible batteries include: 1) constructing freestanding electrodes using carbon nanotubes, graphene or polymers [5–10]; 2) building a strong lamination that can withstand the mechanical stress through solid-state design (inorganic solid electrolyte, gel-polymer electrolyte, etc.) [11–14]; 3) smart engineering design so the electrochemically active layers are at a reduced-strain position [15–17].

One common issue with most reported flexible battery design is that the energy density and specific energy are low, largely because single layer, low areal-capacity loading electrodes are used. Notably, in high loading electrodes or multi-layer stack design, the strain inside the electrodes and at the interfacial regions will be substantially higher. There have been some reports of high specific energy designs [18–21]. However, the values in most of the reports are based on active mass or electrode mass without projection on the total available energy from the system point of view. Highly porous carbon electrodes also greatly penalize energy density of the cells. In addition, the cells were mostly packed in polymer based thin films such as PDMS (polydimethylsilioxane). Despite being light weight, these packaging materials are impractical in real applications due to their high moisture permeation rate [8,10,22].

Structural batteries acting both as power sources and structural

* Corresponding author at: Energy and Environment Directorate, Pacific Northwest National Laboratory, P.O. Box 999, Richland, WA 99352, United States.
E-mail addresses: Zhiqun.Deng@pnnl.gov (Z.D. Deng), jie.xiao@pnnl.gov (J. Xiao).

https://doi.org/10.1016/j.nanoen.2017.11.046
Received 23 October 2017; Received in revised form 16 November 2017; Accepted 17 November 2017
Available online 21 November 2017
2211-2855/

components can improve system-level efficiency by reducing redundancy between sub-systems. Such concept has been successfully applied in electric-propelled unmanned air vehicles (UAVs) and marine systems [23,24]. In this paper, we discuss the fundamental issues when designing structural microbatteries, i.e., tubular-shape microbatteries, and demonstrate the employment of the high-energy microbattery to power real acoustic micro transmitters with sufficiently long cell lifespan. Acoustic transmitters are typically implanted into the body of aquatic animals to monitor the behavior, movement, habitat use, and survival of the tagged animals [25]. The custom designed tubular microbattery improves device integration and space utilization. Design principles that enable high energy tubular batteries include flexible high-loading cathodes and stress management at the cell layers and packaging. Tubular batteries in one of the configurations (4.8 mm in outer diameter) possess an energy density of 916 Wh L^{-1} and specific energy of 550 Wh kg^{-1} excluding packaging (286 Wh L^{-1} and 181 Wh kg^{-1} including packaging), despite having a volume of only 48 mm^3. The construction allows flexible design of battery parameters as we show that the thickness and radius of the tubular batteries can be easily customized.

2. Experiment

The preparation details of tubular batteries are shown as follows: the cathode preparation was similar to the procedure in our previous report [26]. The laminated cathode was 120 μm thick. A 127 μm Li foil was used as anode. A separator bag with two pockets (Fig. 1) was made from polypropylene (PP) separator (Celgard 2500, 25 μm). For all cells, the separator bag was 1 mm longer than the cathode and 2 mm longer than the anode. The electrodes and the separator are then assembly as shown in Fig. 1 and placed in the Al laminated bag. The Al laminated packing film was supplied by Dai Nippon Printing (DNP) Co. A liquid electrolyte (1 M $LiPF_6$ in ethylene carbonate (EC)/dimethyl carbonate (DEC), volume ratio 3:7) was injected. The bag was then heat-sealed with 2 mm sealing margin on all sides under partial vacuum. The assembly process was carried out in a dry room with a dew point of −50 °C. All components were thoroughly dried in vacuum at 65 °C prior to use. The flat pouch cells were rolled into tubular cells of different diameters on a metal rod. Constant pressure was applied during the rolling process.

To observe the lamination inside the tubular cell, dummy dry cells (no electrolyte injection) were embedded in epoxies and polished to reveal the cross section of the lamination. An optical microscope was used to investigate the structure and microstructure of the battery and battery layers.

For electrochemical testing, A CH instrument (Model 6005D) was used to measure the impedance spectra over a frequency range of 100 kHz to 1 Hz with voltage modulation of 5 mV. Prior to the impedance measurement, the cells were activated by discharging at 1 mA for 3 min (corresponding to 1% of the cell capacity) and allowed to equilibrate for at least one hour. A Landt instrument (CT2001A) was used to discharge the cells to 1.5 V at various constant currents.

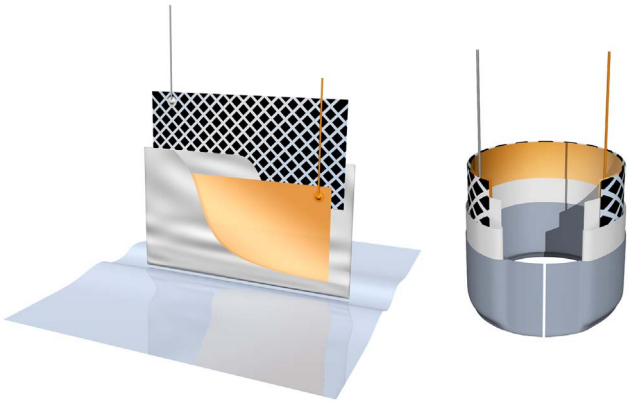

Fig. 1. Schematics of fabrication procedures of tubular batteries.

Acoustic transmitter prototypes powered by the tubular battery were fabricated. The two leads of the battery were first attached to the circuit board (with the piezoelectric transducer already attached to the circuit board) of the transmitter by soldering. The circuit board was then pushed inside the tubular battery. For encapsulation, the transmitters were placed into the cavities of a plastic injection mold. The shape of the cavities defined the final shape of the transmitter. Insulating epoxy (3 M Electrical Resin 5) was then injected into the mold by an air sealant gun and flowed through the cavity before exiting the mold. The injection was kept continuing until no air bubbles was observed exiting the mold. The mold was kept closed at room temperature for 24 h for the epoxy to cure. The transmitter was then removed from the mold and polished to achieve a smooth finish. Lastly, a 25-μm layer of Parylene-C was coated on the transmitter to serve as a water-proof and biocompatible layer. To verify the battery capacity, the service life of two prototype samples of this transmitter was tested in water inside a tank by transmitting an acoustic signal every 3 s. Each transmission consumed about 24 μJ of energy and was detected by two hydrophones (Model SC001, Sonic Concepts Inc., Bothell, Washington, USA) placed inside the tank.

3. Results and discussion

3.1. Electrode preparation

Since the transmitter is a burden to tagged animals in biology studies, high energy density are of paramount importance to the battery design. We choose the CF_x (carbon fluoride, x ≈ 1)/Li battery chemistry as it has one of the highest energy densities and use a high electrode loading of 18 mg cm^{-2}. CF_x is mostly used in low/intermediate power application due to the intrinsic kinetics limitation of the material [27]. Electrodes with smaller CF_x particles generally exhibit better rate capability and higher discharge voltage plateau. In the acoustic transmitters, the power of the transmitter is directly related to the power of the batteries. We therefore chose nanosized CF_x as the active material to maximize power. However, the nanosized particles of CF_x also makes it very challenging to prepare high loading and thick electrodes due to the huge surface area of nanoparticles, a common issue with nano materials for batteries [28]. Another drawback of the coating method is that the bonding between electrode film and Al foil cannot withstand severe bending. To understand why delamination occurs between the coated film and the current collector, it is useful to examine a simple model of a bonded bilayer structure (Fig. 2a). Based on mechanical analysis, the horizontal shear stress τ_h developed at the bilayer interface when a bonded bilayer structure is subjected to a transverse load of F, causing a deflection of δ, is proportional to δ and t^2, and inversely proportional to L^3. (Appendix A)

$$\tau_h = \frac{3E\delta t^2}{L^3}$$

Where δ, t and L are as shown in Fig. 1. E is the Young's modulus of the bilayer structure. The shear stress is sensitive to the bending radius and the thickness of the bilayer. This is why peeling and cracking issues are common for thick electrodes at small bending radius. To minimize stress between the Al current collector and the electrode film, we adopt Al grids loaded with cathode film, a method usually applied in preparing oxygen electrodes for Li-O_2 batteries [29]: mixture of CF_x, conductive carbon and PTFE binder is passed through a rolling mill to form a freestanding film, which is then laminated onto carbon-coated Al grids by hot-pressing (Fig. 1). This design endows great flexibility to the cathode even at a high loading of 18 mg cm^{-2} and electrode density of 1.5 g cm^{-3}. To maximize the packing of CF_x, the content of carbon additive and binder are restricted to 7% and 5%, respectively. The

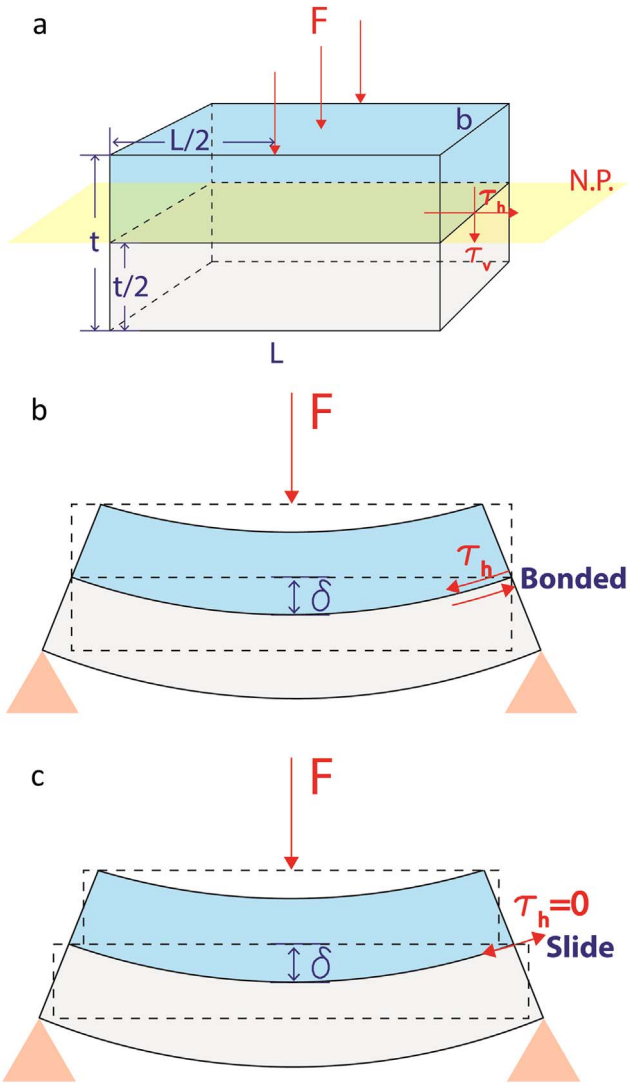

Fig. 2. Schematics of a simple bending model of a bilayer structure. Dimensions and horizontal shear stress of a bonded bilayer structure subjected to a transverse load F: a) 3D view; b) front view. c) Zero horizontal shear stress of a freely-sliding bilayer structure subjected to a transverse load F.

carbon coating on the Al grids is necessary to reduce contact resistance between the electrode film and the current collector. Since the cathode film is loaded into the Al grid, bending of the cathode causes little stress at the cathode/current collector interface.

3.2. Stress management

Aside from stress management at the electrode level, it is also important to minimize stress between the cell layers (cathode/separator and separator/anode). In some flexible battery design, the battery layers are bonded so they may withstand small shear stress. However, similar to the design of coated cathode film on Al foil, delamination is likely to occur in thick battery stacks under small bending radius. In our design, the cell layers are allowed to slide freely against each other so the shear stress at the interface is zero (Fig. 2c). To avoid potential shorting risk after the battery is rolled into a tubular shape, the Li foil is intentionally smaller than the cathode.

One challenge with the design of freely sliding cell stack is keeping the layers well laminated. This is achieved by maintaining compressive stress over the cell layers. The compressive stress comes from 1) atmospheric pressure; 2) structural aspect of the packaging materials. The atmospheric pressure arises from the fact that the battery was sealed under partial vacuum. This is common in pouch-type batteries. The second contributor is unique to the tubular battery design. The aluminum multi-layer laminated film, widely used for packaging pouch cells, was chosen for its unique mechanical property. The film has a polymer-Al-polymer sandwich structure. The 40 μm Al layer largely determines the overall mechanical strength and transverse gas permeability. In the previous model (Fig. 1), it is assumed that the materials are rigid, i.e., the layer can support transfer of force internally, therefore support shear stress. In this case, there is no vertical compressive stress under bending conditions but only shear stress. In the other extreme case, i.e., the materials are flexible, vertical compressive stress (σ_v) is developed where the bending load is applied. The Al laminated film can be considered as semi-rigid, so both compressive and shear stress are present during the rolling process, keeping the battery layers laminated (Fig. 2). The packaging film is plastically deformed. Due to the semi-rigid nature of the film, the film maintains its shape and compressive stress on the cell layers even when the bending force is released at the end of rolling process.

The feasibility of this type of packaging material has been demonstrated in curved batteries commercialized by LG Chem, Samsung, etc [30–32]. In their process, flat pouch cells are deformed and curved using a curve forming apparatus under controlled pressure and heat. However, the curvature in their cells is much smaller than that required by our tubular batteries. The importance of the unique mechanical property of the 40-μm Al laminated film can be further demonstrated by a comparison with tubular batteries packaged with 10-μm Al laminated film (Bemis Company, Inc. thickness here only refers to Al layers in the packaging materials). Although the film reduces packaging weight and volume, it lacks strength to mechanically support the tubular structure. Buckling of the packaging film on the inside of the tubular structure was observed after rolling since the film cannot support horizontal compressive stress (σ_h) developed due to bending (Fig. 3). In the region of buckling, vertical compressive stress that keeps cell layers laminated is lost and the discharge shows an unstable voltage profile.

Fig. 4 shows the cross-sectional optical image of a dummy tubular battery packaged using the 40-μm Al laminated film. A 10 mm × 15 mm (5 × 10 mm for the cathode) flat pouch cell was rolled into a tube of 4.8 mm in outer diameter. The Al laminated film consists of an aluminum layer of 40 μm thick and multiple polymer layers with various functions (scratch protection, adhesion, heat-sealing, etc.). In Fig. 4, the bright continuous layers are the Al layers from the packaging materials. From the outer Al layer to the inner Al layer, the stacks are heat-sealable polymer, PP separator, cathode, PP separator, Li metal, PP separator, heat-sealable polymer. Bright islands in the cathode are Al grid. It can be seen that all the layers were tightly laminated and follow a smooth curve of the battery shape. No buckling was observed on the inner curve of the packaging film, suggesting that the film is indeed semi-rigid and supports horizontal compressive stress. This well-laminated battery layers are indicative of uniform vertical compressive stress across them. It should be noted that the thickness of the cell layer

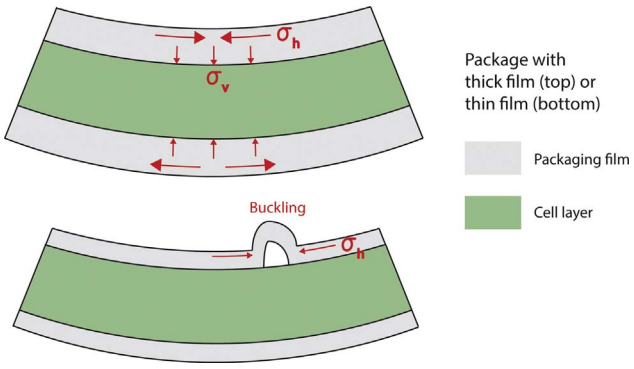

Fig. 3. Schematics of tubular battery packaged with thick or thin packaging films.

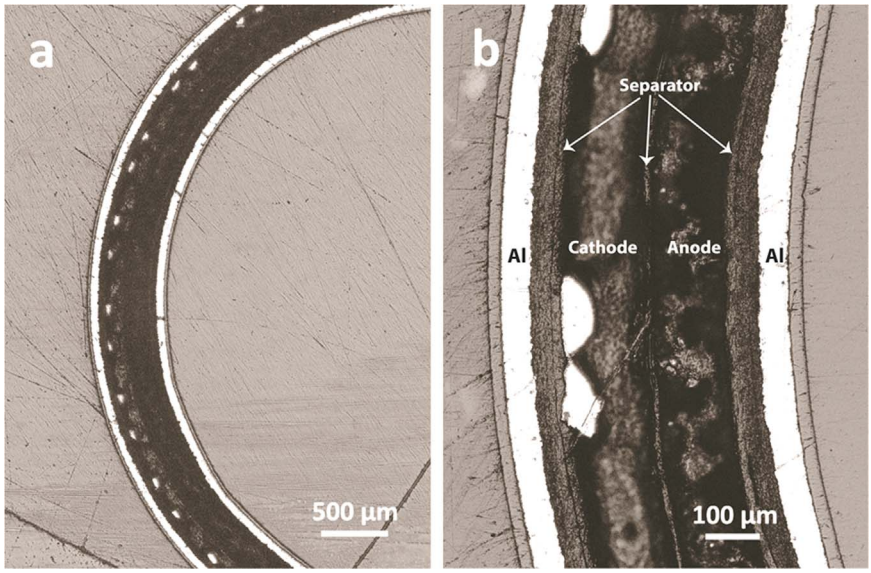

Fig. 4. Cross-sectional optical images of a tubular battery at low magnification (a) and high magnification (b).

is 60% of the total battery thickness, highlighting the necessity of relatively thick packaging film for mechanical support in structural batteries.

3.3. Electrochemical understanding

Impedance spectra and discharge profiles (Fig. 5a and b) were compared for cells with 10 mm × 5 mm cathodes before and after rolled into tubes of outer diameter 4.8 mm. A typical impedance spectrum has one depressed semicircle and a diffusion tail at the low frequency end. The semicircle has contributions from charge transfer reactions at both electrodes and solid electrolyte interface (SEI) on the lithium metal. It is difficult to separate different contributions so we will simply treat it as a single charge transfer resistance. The left intercept of the semicircle is attributed to the Ohmic resistance of the cells including solution resistance and lead resistance. Remarkably, the charge transfer resistance of flat pouch cells was reduced after rolled into tube shape. The Ohmic contribution was relatively the same. The phenomenon that the cell impedance decreases with increasing stack pressure has been well documented, although the exact mechanism to this phenomenon is still under debate [33–35]. We speculate that compressive stress improves contact between and/or within the cell layers and hence reduces impedance. It follows that the reduction of cell impedance after rolling indicates increased stack pressure in the cell. This observation indirectly corroborates our conclusion that the cell stack was under additional compressive pressure from the packaging film under bending conditions, aside from the atmospheric pressure.

The discharge profiles and discharge capacities of flat cells and tubular cells are nearly identical. Therefore, the process of rolling flat cells into tube shape has no negative impact on the utilization of active materials regardless of the discharge current densities. In fact, it is consistently observed that tubular cells have smaller polarization and slightly higher discharge capacity than flat cells, which is consistent with the impedance analysis. At a weight of 76 mg and a volume of 48 mm^3, the tubular battery delivers a discharge capacity of 5.5 mAh at a C/5 rate. The energy density and specific energy are about 915 Wh L^{-1} and 550 Wh kg^{-1} excluding the packaging materials. If the

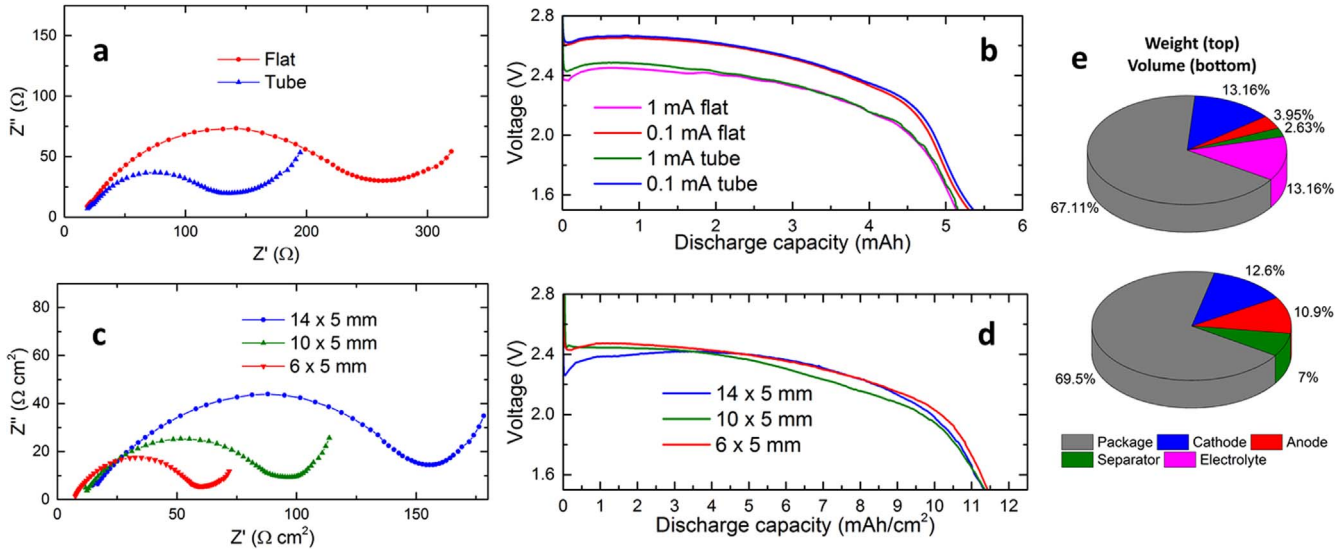

Fig. 5. a) Impedance spectra and b) discharge profiles at a discharge current of 0.1 mA and 1 mA for cells with 5 mm × 10 mm cathodes before and after rolled into tube shape; c) impedance spectra and d) discharge profiles with a current density of 2 mA/cm^2 for tubular cells with different cathode sizes. e) Weight and volume distribution of a typical tubular battery (O.D., 4.8 mm).

packaging weight and volume are included, the energy density and specific energy drop to 286 Wh L^{-1} and 180 Wh kg^{-1}. Indeed, as it can be seen from the weight and volume distribution (Fig. 5e), the packaging contributes about 2/3 of the overall weight and volume. Clearly, reducing the packaging weight and volume remains the most critical factor in future research of practical microbatteries.

To further understand the process of rolling on the electrochemical performances of the cells, tubular batteries with different cathode sizes (14 mm, 10 mm and 6 mm in length) and hence different diameters were compared (Fig. 5c and d). For fair comparison, the impedance spectra were normalized by the area of cathodes and the same discharge current density was used to discharge the cells. The normalized impedance varies following the order of radius of the cells. This observation confirmed that the tubular design reduces cell impedance. The normalized discharge capacities of tubular battery with different radius were nearly identical. Remarkably, tubular batteries with of stack thickness of 0.5 mm and a bending radius 1.8 mm still retain their normal function.

The limits of bending radius and stack thickness are determined by the ability of the packaging film to accommodate compressive and tensile stress at the inner and outer surfaces of the tube. If the outer diameter is D and the stack thickness is T, we can define a dissimilar factor

$$\Delta D = 2T/D.$$

ΔD for the 6 mm-cathode cell is 28.5%, which means that the two sides of packaging film initially of equal lengths will have to accommodate 28.5% of length difference after rolling. We observe some buckling in these cells marking the limit of the design. To extend the limit, we believe design modifications such as pre-forming cups on the outer packaging film or rolling at higher pressures and elevated temperatures are necessary.

3.4. Post mortem analysis

Lithium metal anode used in this work is ca. 127 μm corresponding to an areal capacity of ca.25 mAh/cm^2, while the cathode is about 10 mAh/cm^2. Accordingly, the negative/positive (N/P) ratio is 2.5 for this primary cell. Although reducing the thickness of lithium metal may further reduce the weight and volume slightly, a high N/P ratio is recommended due to the non-uniform stripping process of Li metal during cell discharge. Fig. 6 shows the optical images of Li metal after discharge. Many pits show up on the surface of Li anode after discharge (Fig. 6a). The cross-sectional image (Fig. 7b) clearly indicates that the stripping of Li metal from the anode is quite inhomogeneous. Some parts of Li are intact, whereas other locations were deeply "corroded" 90 μm towards the bulk Li. This observation suggests that the excessive amount of Li on the anode functions as a current collector to ensure the smooth current flow. If thin Li metal is used, the deep stripping process easily leads to the "cracking" of the whole Li anode leading to the fast cell termination. The fundamental reason for the non-uniform reaction of Li during discharge is related with the different properties of original solid electrolyte interface (SEI) formed at various locations cross the anode surface in the beginning. Although this tube battery is a primary cell that only depletes Li metal during discharge, the discovery here provides important insights for the rational design of rechargeable Li metal batteries. Li metal itself probably cannot be a durable current collector in a practical cell, even if excessive amount of Li is used. After repeated cycling, it is highly possible that some of "holes" formed will directly penetrate the whole Li metal and the continuous electronic conductivity will easily be lost on the anode side. For rechargeable Li metal batteries, a very light but highly conductive current collector for Li metal anode will still be necessary to enhance the cycling stability of Li metal without increasing the "dead" weight too much in the cell.

3.5. Device integration

To investigate the real-life performance of the tubular battery in a small electronic device, the tubular battery of 4.8 mm diameter was incorporated in an underwater acoustic transmitter, in which the electronic components of the transmitter were tucked inside the hollow space of the tube (Fig. 7a). The transmitter consisted of a piezoelectric transducer for signal transmission, a circuit board with the controlling circuit and the tubular battery as the power source. The service life of two prototype samples of this transmitter was tested in water at a ping rate of 3 s Fig. 7b demonstrates an actual waveform signal transmitted by the prototype transmitter and received by a hydrophone. The waveform was the amplified output voltage of the hydrophone as a function of time, which contained the identification code of the transmitter. Based on the nominal capacity of 11 mAh, the projected service life at a 3-second ping rate was about 145 days. The actual service life of the two samples were measured to be 140 and 165 days, respectively, consistent with the projected value. To our knowledge, this is the first demonstration of functional micro electronic device powered by a tubular battery.

4. Conclusions

The rational design and the fundamental issues associated with high energy tubular microbatteries has been discussed. Stress generated during the rolling process has been managed at different levels from the electrode fabrication to cell-stacking and packaging. Especially, selection of a semi-rigid packing material that is rigid enough to act as mechanical support while malleable enough to accommodate large mechanical stress under severe bending conditions. Electrochemical evaluations of as-designed cell proved that the rolling process has no detrimental effect on the battery performances. Conversely, the higher stack pressure in tubular batteries endows small beneficial effects to the cell impedance. After deep discharge, Li metal has been found to be stripped non-uniformly indicating the significant surface properties at

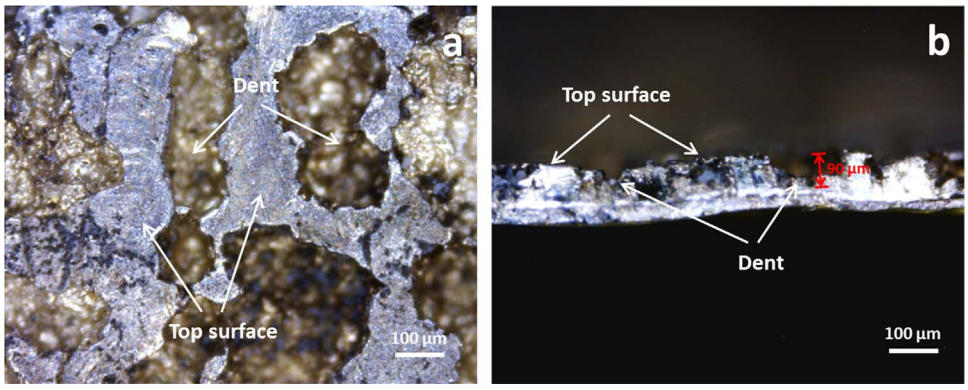

Fig. 6. Optical images of the deeply stripped Li metal: a) top view & b) cross sectional view. The areal capacity of reacted Li metal is ca. 10 mAh/cm^2 at a rate of 2 mA/cm^2.

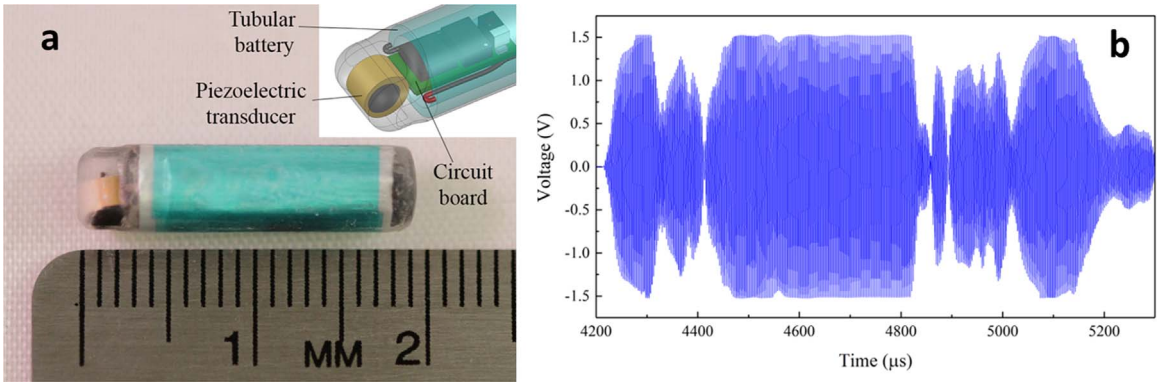

Fig. 7. (a) A Photo and a CAD drawing of the prototype transmitter that used the tubular battery. (b) Acoustic waveform transmitted by the prototype transmitter that used the tubular battery as the power source.

different locations of Li metal. The practicality of the tubular battery as structural batteries has been successfully demonstrated in a fully-integrated acoustic device. The findings in the study provide useful guidelines for designing tubular or other structural batteries.

Acknowledgment

The study was funded by the U.S. Department of Energy (DOE) Water Power Technologies Office and the U.S. Army Corps of Engineers (USACE), Portland District. The authors would like thank Brad Eppard, Scott Fielding and Ricardo Walker of USACE and Jocelyn Brown-Saracino, Dana McCoskey, and Hoyt Battey of DOE for their support. The study was conducted at Pacific Northwest National Laboratory, which is operated by Battelle for DOE.

Notes

The authors declare no competing financial interest.

Appendix A

Derivation of horizontal shear stress

Consider a bonded bilayer structure under bending conditions with simple support on both ends. The two layers are of equal thickness. A transverse load F is applied to the center (along the lateral direction) of structure. It is assumed that 1) the neutral plane coincides with the boundary of the two layers; 2) the two materials are homogeneous and linearly elastic; 3) the deflection of the structure is small.

The load required to bend the bilayer to a deflection of δ is

$$F = 48EI\delta/L^3$$

Where E is the Young's modulus of the bilayer structure and I is moment of inertia.

The vertical shear force at any point of the structure can be determined from the shear force diagram

$$V = F/2$$

In solid mechanics, the vertical shear stress distribution over the cross section is parabolic

$$\tau_v = \frac{V}{2I}\left(\frac{t^2}{4} - y^2\right)$$

Where y is the distance between the shear plane and the neutral plane, which is zero in this case. The horizontal shear stress is equal to the vertical shear stress at any particular point

$$\tau_h = \tau_v = \frac{3E\delta t^2}{L^3}$$

References

[1] F. Schlachter, Proc. Natl. Acad. Sci. USA 110 (2013) (5273-5273).
[2] H. Gwon, J. Hong, H. Kim, D.H. Seo, S. Jeon, K. Kang, Energy Environ. Sci. 7 (2014) 538–551.
[3] G.M. Zhou, F. Li, H.M. Cheng, Energy Environ. Sci. 7 (2014) 1307–1338.
[4] Y.H. Hu, X.L. Sun, J. Mater. Chem. A 2 (2014) 10712–10738.
[5] S.H. Liu, Z.Y. Wang, C. Yu, H.B. Wu, G. Wang, Q. Dong, J.S. Qiu, A. Eychmuller, X.W. Lou, Adv. Mater. 25 (2013) 3462–3467.
[6] H. Gwon, H.S. Kim, K.U. Lee, D.H. Seo, Y.C. Park, Y.S. Lee, B.T. Ahn, K. Kang, Energy Environ. Sci. 4 (2011) 1277–1283.
[7] V.L. Pushparaj, M.M. Shaijumon, A. Kumar, S. Murugesan, L. Ci, R. Vajtai, R.J. Linhardt, O. Nalamasu, P.M. Ajayan, Proc. Natl. Acad. Sci. USA 104 (2007) 13574–13577.
[8] N. Li, Z.P. Chen, W.C. Ren, F. Li, H.M. Cheng, Proc. Natl. Acad. Sci. USA 109 (2012) 17360–17365.
[9] J.Z. Wang, S.L. Chou, J. Chen, S.Y. Chew, G.X. Wang, K. Konstantinov, J. Wu, S.X. Dou, H.K. Liu, Electrochem. Commun. 10 (2008) 1781–1784.
[10] L.B. Hu, H. Wu, F. La Mantia, Y.A. Yang, Y. Cui, ACS Nano 4 (2010) 5843–5848.
[11] S.H. Lee, P. Liu, C.E. Tracy, D.K. Benson, Electrochem. Solid State 2 (1999) 425–427.
[12] M. Koo, K.I. Park, S.H. Lee, M. Suh, D.Y. Jeon, J.W. Choi, K. Kang, K.J. Lee, Nano Lett. 12 (2012) 4810–4816.
[13] Z.Q. Wang, Z.Q. Wu, N. Bramnik, S. Mitra, Adv. Mater. 26 (2014) 970–976.
[14] E.H. Kil, K.H. Choi, H.J. Ha, S. Xu, J.A. Rogers, M.R. Kim, Y.G. Lee, K.M. Kim, K.Y. Cho, S.Y. Lee, Adv. Mater. 25 (2013) 1395–1400.
[15] Y.H. Kwon, S.W. Woo, H.R. Jung, H.K. Yu, K. Kim, B.H. Oh, S. Ahn, S.Y. Lee, S.W. Song, J. Cho, H.C. Shin, J.Y. Kim, Adv. Mater. 24 (2012) 5192–5197.
[16] S. Xu, Y.H. Zhang, J. Cho, J. Lee, X. Huang, L. Jia, J.A. Fan, Y.W. Su, J. Su, H.G. Zhang, H.Y. Cheng, B.W. Lu, C.J. Yu, C. Chuang, T.I. Kim, T. Song, K. Shigeta, S. Kang, C. Dagdeviren, I. Petrov, P.V. Braun, Y.G. Huang, U. Paik, J.A. Rogers, Nat. Commun. 4 (2013).
[17] Y. Liu, S. Gorgutsa, C. Santato, M. Skorobogatiy, J. Electrochem. Soc. 159 (2012) A349–A356.
[18] Q.C. Liu, T. Liu, D.P. Liu, Z.J. Li, X.B. Zhang, Y. Zhang, Adv. Mater. 28 (2016)

8413–8418.
[19] Y.X. Zeng, X.Y. Zhang, Y. Meng, M.H. Yu, J.N. Yi, Y.Q. Wu, X.H. Lu, Y.X. Tong, Adv. Mater. 29 (2017).
[20] X.L. Dong, L. Chen, X.L. Su, Y.G. Wang, Y.Y. Xia, Angew. Chem. Int. Ed. 55 (2016) 7474–7477.
[21] Z.N. Deng, H. Jiang, Y.J. Hu, Y. Liu, L. Zhang, H.L. Liu, C.Z. Li, Adv. Mater. 29 (2017).
[22] Y.H. Zhang, M. Ishida, Y. Kazoe, Y. Sato, N. Miki, IEEJ Trans. Electr. Electron. 4 (2009) 442–449.
[23] J.P. Thomas, S.M. Qidwai, W.R. Pogue, G.T. Pham, J. Compos. Mater. 47 (2013) 5–26.
[24] J.P. Thomas, M.A. Qidwai, JOM-Us 57 (2005) 18–24.
[25] Z.D. Deng, T.J. Carlson, H. Li, J. Xiao, M.J. Myjak, J. Lu, J.J. Martinez, C.M. Woodley, M.A. Weiland, M.B. Eppard, Sci. Rep.-Uk 5 (2015).
[26] H.H. Chen, S. Cartmell, Q. Wang, T. Lozano, Z.D. Deng, H.D. Li, X.L. Chen, Y. Yuan, M.E. Gross, T.J. Carlson, J. Xiao, Sci. Rep.-Uk 4 (2014).
[27] Y.X. Wang, B. Liu, Q.Y. Li, S. Cartmell, S. Ferrara, Z.Q.D. Deng, J. Xiao, J. Power Sources 286 (2015) 330–345.
[28] D.P. Lv, J.M. Zheng, Q.Y. Li, X. Xie, S. Ferrara, Z.M. Nie, L.B. Mehdi, N.D. Browning, J.G. Zhang, G.L. Graff, J. Liu, J. Xiao, Adv. Energy Mater. 5 (2015).
[29] J. Xiao, D.H. Mei, X.L. Li, W. Xu, D.Y. Wang, G.L. Graff, W.D. Bennett, Z.M. Nie, L.V. Saraf, I.A. Aksay, J. Liu, J.G. Zhang, Nano Lett. 11 (2011) 5071–5078.
[30] E.Y. Goh, B. Choi, H.M. Lee, H.C. Jung, US Patent, 0090236 A1, 2014.
[31] R.C. Bhardwaj, J. Raff, S.R. McClure, E.L. Wang, T. Hwang, US Patent, 0136967 A1, 2013.
[32] E.Y. Goh, B. Choi, B.I. Lee, H.R. Jung, US Patent, 0097615 A1, 2011.
[33] M. Gaberscek, J. Moskon, B. Erjavec, R. Dominko, J. Jamnik, Electrochem. Solid State 11 (2008) A170–A174.
[34] J.M. Atebamba, J. Moskon, S. Pejovnik, M. Gaberscek, J. Electrochem. Soc. 157 (2010) A1218–A1228.
[35] K.J. Nelson, G.L. d'Eon, A.T.B. Wright, L. Ma, J. Xia, J.R. Dahn, J. Electrochem. Soc. 162 (2015) A1046–A1054.